Article

Effect of Geo-Material on Dynamic Response of Tunnel Subjected to Surface Explosion

Jagriti Mandal * and Manmohan Dass Goel (ID)

Department of Applied Mechanics, Visvesvaraya National Institute of Technology, Nagpur 440010, India
* Correspondence: jagritimandal@students.vnit.ac.in

Abstract: Prime materials involved in a problem such as underground structures are concrete, reinforcement steel, and geo-material surrounding the tunnel. Among these three materials, concrete and steel are manufactured materials and their properties can be controlled up to a certain extent. However, geo-material is a naturally occurring material whose constitutive properties vary from region to region, making it highly unpredictable. Findings from one study cannot be applied to other geotechnical problems directly, especially in the case of tunnels subjected to surface explosions. The blast wave generated has to travel through the geo-material before it interacts with the tunnel. As the shock wave propagates radially, its characteristics are likely to be altered by the geo-material. Limited study has been carried out considering this problem. In the present study, the effect of various types of geo-material on the blast response of tunnels subjected to surface explosions is investigated. Finite element analysis has been carried out using LS-DYNA®, wherein the problem has been modeled using the multi-material arbitrary Lagrangian–Eulerian (MM-ALE) method. Materials with fluid behavior such as air, explosives, and soil are modeled using ALE formulation. Other materials including tunnel lining, reinforcement steel, and rock are modeled using Lagrangian formulation. Blast loading is simulated using the Jones–Wilkins–Lee (JWL) equation of state. Geo-materials considered for the comparative study are sandy loam, saturated clayey soil, sandstone, and granite. Vertical displacement measured at the crown of the tunnel is used to determine the response of the tunnel. Sandy loam soil, being a highly compressible soil, exhibits non-linear and fluid-like behavior under high-strain loading such as explosions. Tunnels undergo extreme deformation in the case of sandy loam soil and clayey soil compared to rock cases. Further, the effect of saturation in sandy loam on tunnel stability is studied. It is observed that with the increase in saturation of soil, more blast energy is transmitted to the structure, which results in higher deformation. Lastly, the effect of the weathering of rock on the tunnel's response is investigated in the case of sandstone and granite. It was observed that weathering in rock led to more displacement of tunnel crown when compared to intact rock.

Keywords: MM-ALE; rock; sandy loam; weathering; compressibility; tunnel

1. Introduction

The prime materials involved in a problem such as underground structures are concrete, reinforcement steel, and geo-material surrounding the tunnel. Among these three materials, concrete and steel are manufactured materials, and the properties which define their behavior can be controlled up to a certain extent. However, geo-material is a naturally occurring material whose constitutive properties vary from region to region, making it highly unpredictable. Findings from one study cannot be applied to other geotechnical problems directly, especially in the case of a tunnel subjected to an external explosion. In the surface explosion, the blast wave generated has to travel through the geo-material before it interacts with the tunnel. As the shock wave propagates radially, its characteristics are likely to be altered by the geo-material. The wave may undergo attenuation or amplification; however, the degree of change depends on many factors such as type of

geo-material, porosity, degree of saturation, degree of weathering, strength characteristics, etc. Although blast analysis of underground structures has been carried out with different types of geo-materials, limited study has been done which digs deep into the influence of individual factors. Besides the shock-wave generation aspect of a surface explosion, crater formation is another important phenomenon that plays an important role, especially if the structure is shallow-buried. Crater formation involves erosion and rapid compression of material which could be detrimental to a structure if the cover depth is shallow. This necessitates the research on crater formation and the factors that can potentially influence the shape and size of craters.

Most of the studies conducted employ numerical simulation, since performing an experimental test for problems similar to the current study is often not feasible. Numerical simulation has proven to be a reliable tool in solving non-linear dynamic problems; however, there are still complexities present in dealing with high-strain rate, large-deformation problems. Simulating explosions leading to blast load propagation and rapid crater formation in geo-material involves high-strain-rate loading of material, large plastic deformation, triggering liquefaction of material, and erosion of material. All these complex processes are highly transient and happen simultaneously, which often makes the simulation cumbersome. Numerical instability and abruption of analysis are frequently caused by extreme mesh distortion caused by substantial deformation. The use of a hybrid model with two or more different element formulations has been shown to reduce large deformation errors during simulation. Many coupled approaches to model blast loads have been developed in recent years. The coupled Lagrangian–Eulerian approach, for example, has been effectively employed to model a tunnel subjected to a surface explosion [1–7].

Sandy soils and clay have been widely considered for the study of tunnels' responses to surface explosions, since they are found commonly in many parts of the world [1,3,5–15]. Sandy soils are highly compressible in nature, whereas clay behaves comparatively stiff. Hard and soft rock are also encountered in the strata and have been considered in the study [16–21]. However, these studies have been conducted separately with different geometrical details, boundary conditions, and other influential factors. There is no common basis for comparison, which makes it challenging to determine which geo-material is more favorable for an underground structure under blast loads. Thus, a comparative study is needed where the effect of different geo-materials on blast-wave propagation, crater formation, and dynamic response of the structure are investigated.

Hence, this study aims at investigating the behavior of tunnels buried in various geo-materials subjected to surface explosions. The geo-materials considered in the study are sandy loam soil, clayey soil, sandstone, and granite. The study entails a general comparison between soils and rocks and studying the effects of degree of saturation in soil and degree of weathering in rocks. The compressibility of soil has been assumed as a measure of degree of saturation in soil, considering the fact that water predominantly influences the compression capacity of the soil. Further, the compressibility of soil is controlled with the help of a hydrostatic compression curve, which is input in a tabulated form into the material model.

2. Geometrical and Finite Element Details

A box-shaped tunnel of width 6 m and height 5 m has been considered for the present investigation. The thickness of the tunnel lining is taken as 300 mm. The lining is made of reinforced concrete. The reinforcement details are presented in Figure 1.
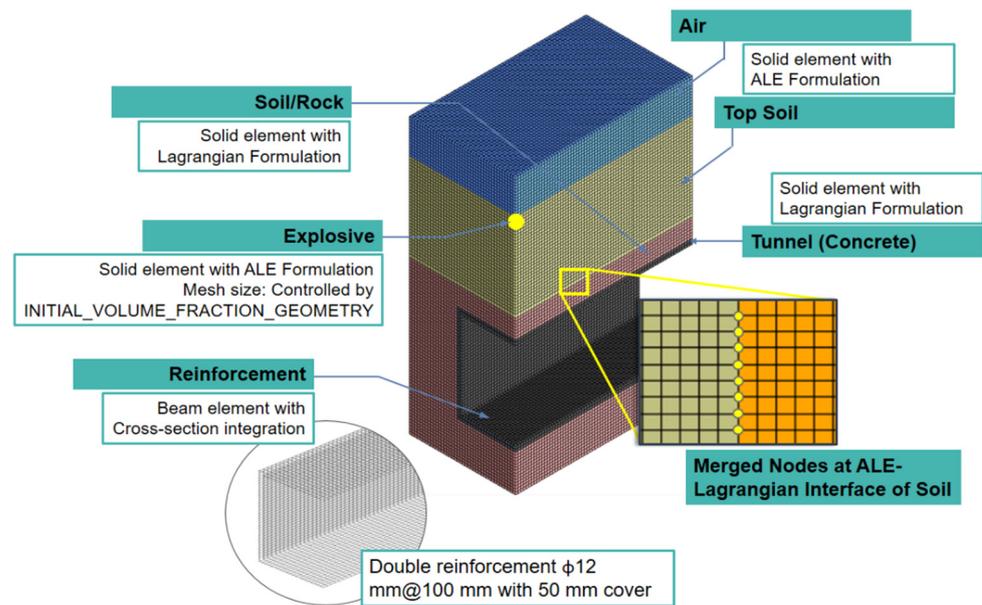
Figure 1. Finite element details of the model with reinforcement details.

A soil cover of 6 m from the crown of the tunnel is assumed. Considering the symmetry of the problem, the model is cut along two symmetrical planes, and symmetrical boundary conditions are applied to the nodes to constrain their lateral movement. A nominal mesh size of 150 mm is chosen from a convergence study where three sizes were considered: 300 mm, 150 mm, and 100 mm. A 2 m high column of air is modeled on top of the soil to accommodate expulsion of ejecta and formation of craters in the soil. The explosive is modeled using the volume fraction geometry method and is located at the interface of soil and air, over the crown of tunnel. Non-reflecting boundary conditions are applied on the outer sides of the soil domain to reduce the reflection of blast waves, which can cause interferences with the results.

Two cases of geo-material formation have been considered in the study. In the first case, the entire geo-material domain is considered to be made of sandy loam soil. In the second case, the geo-material domain is considered to be made of two layers; the top layer is made of sandy loam, which is overlayed on top of rock strata, as shown in Figure 1. The thickness of topsoil in the second case is taken as 5 m. The entire problem has been modeled using the multi-material arbitrary Lagrangian–Eulerian (MM-ALE) method where tunnel, rock, and rebar are modeled using Lagrangian element formulation. Air, soil, and explosive are modeled using ALE element formulation. Lagrangian and ALE elements are coupled using the fluid–solid coupling method. All the materials are modeled using solid elements with reduced integration except for reinforcement. The rebar steel is modeled using beam elements and they are coupled with concrete using a constrained Lagrangian in the solid option.

3. Material Models

3.1. Geo-Materials

A soil and foam material model has been used to simulate the highly compressible nature of sandy loam soil. This model is capable of simulating fluid-like behavior under low yield, which makes it suitable for soft soils such as one considered in the present study. The model is based on a pressure-dependent failure surface incorporating volumetric deformation. The deviatoric behavior of the model is defined by a pressure-dependent perfectly plastic yield function,

$$\varphi = J_2 - \left(a_0 + a_1 p + a_2 p^2 \right) \tag{1}$$

where J_2 is the second deviatoric invariant; a_0, a_1, and a_2 are constants for plastic yield function; and p is mean stress. The compaction and crushing of soil are defined using a hydrostatic compression curve which needs to be input in tabulated form. Compressibility of soil decreases as its degree of saturation is increased. Hence, in this study, the hydrostatic compression curve is used as the measure of the degree of saturation in the soil considered. The properties used to define the behavior of sandy loam soil and saturated clayey soil are given in Table 1. The tabulated data of hydrostatic compressibility are given in Table 2. Three levels of saturation in soil have been considered wherein the degree of saturation increases from sandy loam sample SL1 to sandy loam sample SL3. Sandy loam sample SL2 has a saturation level approximately in the mid-range between SL1 and SL3, and has been taken as a standard sandy loam soil sample for comparison with other geo-materials.

Table 1. Material properties of sandy loam and clayey soils [6,22].

	Sandy Loam	Clayey Soil
Density (kg/m^3)	1255	1963
Shear Modulus (MPa)	1.724	2.524
Bulk Modulus (MPa)	5.516	4673
A0 (MPa^2)	0	0.001
A1 (MPa)	0	0.0049
A2	0.8702	0.0079
Tension Pressure Cutoff (MPa)	0	−0.05

Table 2. Tabulated data of hydrostatic compression curve [6,22].

Sandy Loam Volumetric Strain	Pressure (MPa)	Sandy Loam Volumetric Strain	Pressure (MPa)	Sandy Loam Volumetric Strain	Pressure (MPa)	Clayey Soil Volumetric Strain	Pressure (MPa)
0.05	0.02	0.05	0.02	0.05	0.02	0	0
0.104	0.029	0.1	0.05	0.101	0.061	−0.0216	100
0.157	0.052	0.15	0.07	0.144	0.104	−0.0437	200
0.216	0.085	0.2	0.12	0.184	0.16	−0.0895	400
0.29	0.192	0.25	0.2	0.223	0.232	−0.1374	600
0.338	0.324	0.3	0.34	0.262	0.365	−0.1878	800
0.373	0.466	0.33	0.5	0.279	0.483	−0.2408	1000
						−0.5586	2000
						−1.0272	3000
						−1.938	4000

Rock has been modeled using the Johnson–Holmquist concrete (JHC-2) model. This model was initially developed to simulate concrete under high-strain-rate loading and large deformation. However, since both concrete and rocks are brittle materials with similar fracture mechanisms, this JHC-2 is also used for rock simulation under extreme loads. It uses a three-stage polynomial equation of state to determine the pressure–volumetric strain of material. The three phases considered here are the elastic phase, plastic phase, and compaction phase. It incorporates a damage failure model which is controlled by defining two damage factors. The yield surface of the model is expressed as:

$$\sigma^* = \left[A(1 - D) + BP^{*N} \right] \left(1 + C \ln \dot{\varepsilon}^* \right) \tag{2}$$

where σ^* is the dimensionless equivalent stress and defined as:

$$\sigma^* = \frac{\sigma}{f_c} \tag{3}$$

where σ is the actual equivalent stress; f^c is the quasi-static yield strength; A, B, D, N, and C are the material constitutive model parameters; p^* is the dimensionless pressure and is the ratio of actual pressure to quasi-static yield strength; and ε^* is the ratio of strain rate to

reference strain rate. The value of damage factor D defines the damage accumulation as a percentage of the cohesive strength of the material and varies from 0 to 1, wherein $D = 1$ indicates full damage.

Material parameters of all the rocks considered in the study are listed in Table 3.

Table 3. Material properties of rock mass [23–26].

Parameters	Sandstone	Granite	Weathered Sandstone	Weathered Granite
Density, kg/m^3	2670	2683	1890	2650
Shear Modulus, Pa	1.33×10^{10}	2.20×10^{10}	9.90×10^9	1.19×10^{10}
Normalized Cohesion	0.79	0.79	0.53	0.1
Pressure Hardening Coefficient	1.6	1.6	1.2	2.298
Strain Rate Coefficient	0.007	0.007	0.004	0.007
Pressure Hardening Exponent	0.61	0.61	0.42	1.0344
UCS, Pa	1.21×10^8	1.21×10^8	3.30×10^7	8.34×10^7
Maximum Tensile Hydrostatic Pressure, Pa	8.30×10^6	1.10×10^7	2.86×10^6	5.63×10^6
Quasi-static Reference Strain Rate	1.00×10^{-6}	1.00×10^{-6}	1.00×10^{-6}	1.00×10^{-6}
Minimum Plastic Strain Before Fracture	0.01	0.01	0.01	0.01
Normalized Maximum Strength	7	12	7	7
Crushing Pressure, Pa	5.70×10^8	5.70×10^7	1.30×10^7	2.75×10^7
Crushing Volumetric Strain	0.01	2.50×10^{-6}	0.001	1.88×10^{-6}
Locking Pressure, Pa	8.00×10^8	8.00×10^8	7.80×10^8	8.00×10^8
Locking Volumetric Strain	0.08	0.08	0.1	0.1
Damage Coefficient (D1)	0.04	0.04	0.024	0.0426
Damage Coefficient (D2)	1	1	1	1
Unloading Bulk Modulus, Pa	8.50×10^{10}	8.50×10^{10}	6.30×10^{10}	8.50×10^{10}
Pressure Constant (k2), Pa	-1.71×10^{10}	-1.70×10^{11}	-1.42×10^{11}	-1.71×10^{11}
Pressure Constant (k3), Pa	2.08×10^{10}	2.00×10^{11}	1.69×10^{11}	2.08×10^{11}

3.2. Air

Air has been modeled using the null material model, where its density is taken as 1.29 kg/m^3. This model allows incorporation of equation of states without calculating deviatoric stress. Since the model has zero shear stiffness, it requires appropriate hourglass control to avoid energy loss. For the present study, the hourglass coefficient was taken 0.1. The air has been assumed as an ideal gas and its behavior is controlled using a linear polynomial equation of state, which is governed by the following equation:

$$P = C_0 + C_1\mu + C_2\mu^2 + C_3\mu^3 + \left(C_4 + C_5\mu + C_6\mu^2\right)E \quad (4)$$

Since the air is assumed as an ideal gas here, the gamma-law equation of state has been applied. Based on this law, the pressure (P) equation can be simplified by substituting the coefficients C_0, C_1, C_2, C_3, and C_6 with zero, and coefficients C_4 and C_5 with $(\gamma-1)$. Thus, the expression becomes

$$P = (\gamma - 1)\frac{\rho}{\rho_0}E \quad (5)$$

Here, γ (ratio of specific heat) = 1.4, ρ_0 (initial density of the air) = 1 MPa, and E (internal energy per initial volume) = 0.25 MPa.

3.3. Explosive

For the present study, Tri-nitro-toluene (TNT) is taken as the explosive. The behavior of this explosive is defined using high explosive burn material model and the Jones–Wilkins–Lee equation of state. The pressure generated at any given time by an explosive element is

$$p = FP_{EOS}(V, E) \quad (6)$$

where F is a burn factor that controls the chemical energy generated from detonation; P_{EOS} is the pressure estimated from the JWL equation of state; V is the relative volume; and E is internal energy per unit volume. The value of the burn factor, F, depends on the beta setting. There are two burn options: beta burn, wherein detonation occurs due to volumetric compression; and programmed burn, wherein the detonation is controlled by the INITIAL_DETONATION option, which defines the time and location of detonation. The equation of state is not required when the beta option is set to beta burn. For the study, the beta option was set to default, which incorporated both beta burn and programmed burn options.

The burn factor, F, was taken as the maximum of the two:

$$F = \max(F_1, F_2) \tag{7}$$

where F_1 is for the beta burn option and F_2 is for the programmed burn option,

$$F_1 = \begin{cases} \frac{2(t-t_1)DA_{e,\max}}{3v_e} & if \ t > t_l \\ 0 & if \ t \geq t_l \end{cases} \tag{8}$$

$$F_2 = \frac{1-V}{1-V_{CJ}} \tag{9}$$

Here, t is the current time and t_1 is a lighting time which dictates the initialization phase of denotation simulation. For each explosive element, the distance from its center to the detonation point is divided by the detonation velocity, D, which gives the lighting time. V_{CJ} is the Chapman–Jouguet relative volume; v_e is the element volume; and $A_{e,\max}$ is the maximum element area. On fulfilment of criteria for the beta option, blast energy is released based on the pressure calculated by the JWL equation of state, which is

$$p = A\left(1 - \frac{\omega}{R_1 V}\right)e^{-R_1 V} + B\left(1 - \frac{\omega}{R_2 V}\right)e^{-R_2 V} + \frac{\omega E}{V} \tag{10}$$

The parameters required to model the explosive and its detonation are listed in Table 4, where ρ is density; v_D is the velocity of detonation; P_{cut} is the Chapman–Jouguet pressure; and ω, A, B, R_1 and R_2 are JWL parameters.

Table 4. Material properties for TNT [6].

Parameters	Values
P (kg/m^3)	1630
v_D (m/s)	6930
P_{cut} (MPa)	2.1×10^4
A (MPa)	3.738×10^5
B (MPa)	3.747×10^3
R_1	4.15
R_2	0.9
ω	0.35
V_0	1
E_0 (MPa)	6000

3.4. Tunnel

The tunnel is a composite made of concrete and reinforcement steel bars. These materials are modeled separately as two parts in order to simulate the elastic–plastic nature of reinforced concrete. Reinforcement steel is modelled using a plastic kinematic model with material properties density = 7850 kg/m^3, Young's modulus = 210 GPa, Poisson's ratio = 0.29, and yield and stress = 500 MPa. Concrete is modeled using the Winfrith model, which is based on the shear failure surface and is expressed as

$$F(I_1, J_2, \cos 3\theta) = a\frac{J_2}{(f_c')^2} + \lambda\frac{\sqrt{J_2}}{f_c'} + b\frac{I_1}{f_c'} - 1 \tag{11}$$

Strain softening of concrete is simulated in terms of tensile cracking, which is controlled by defining unconfined tensile strength and crack width at which the tensile strength of concrete will be zero across the crack.

The formulation for crack width is based on the results of experiments conducted by Wittmann in 1988 [27],

$$w = \frac{2G_F}{f_t'} \tag{12}$$

where G_F is specific fracture energy and f_t' is unconfined tensile strength. The material parameters are given in Table 5.

Table 5. Material properties of concrete [6].

Parameters	Values
Density (kg/m^3)	2300
Tangent Modulus (MPa)	2903
Poisson's ratio	0.2
Unconfined Compressive Strength (MPa)	34.48
Unconfined Tensile Strength (MPa)	4
Crack Width (mm)	0.041
Aggregate size (mm)	4.763

4. Validation of Numerical Scheme

The FE modeling approach developed is validated based on crater size. Baker et al. [28] developed an empirical formula based on a series of experimental tests, which can predict the size of the crater formed in geo-materials due to explosions. It is expressed as

$$\frac{R}{d} = f\left(\frac{W^{\frac{7}{24}}}{\sigma^{\frac{1}{6}}K^{\frac{1}{8}}d}\right) \tag{13}$$

Here, W is the explosive charge weight; d is the buried depth of explosive; R is the apparent radius of the crater; σ is the stress factor; and K is the gravitational factor. For validation purposes, a series of numerical simulations were conducted with varying explosive weight and depth of buried explosion. The results were compared with the predicted values of the scaled radius of the crater using the above empirical formula for the corresponding set of explosive charge and depth of burial, as shown in Figure 2. The results agree well with the empirical formula, thus validating the FE modeling scheme.
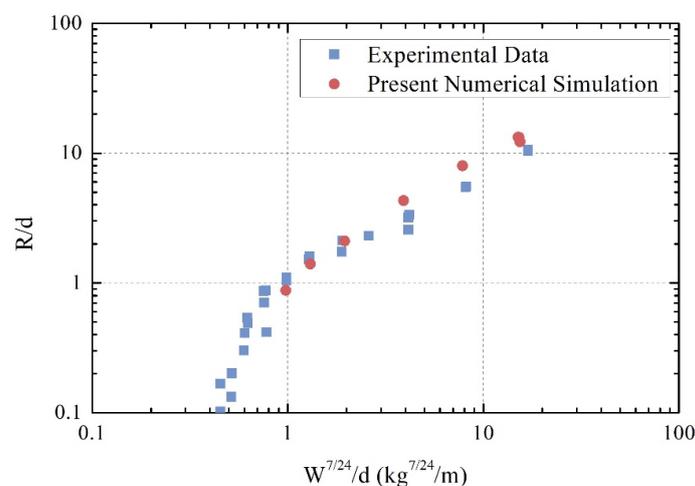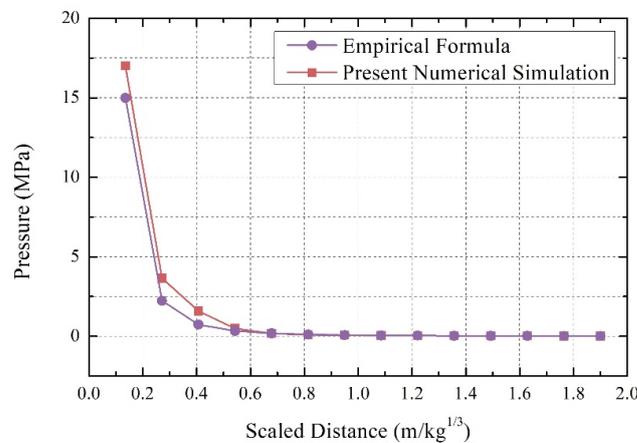

Figure 2. Comparison of numerically obtained crater dimension with experimental results [28].

Ground motion is measured using displacement, peak particle velocity (PPV), and peak particle acceleration (PPA), whereas ground shock is often measured using soil

pressure. Fundamentals of Protective Design for Conventional Weapons (TM5-855-1) [29] is a technical manual published by the United States Army that offers an equation to predict soil pressure (*P*, in MPa) in sandy loam soil for a given charge weight (*W*, in kg) and stand-off distance of explosives (*R*, in m),

$$P = 8.954 f \left(\frac{R}{W^{1/3}} \right)^{-2.75} \tag{14}$$

Here, *f* is the coupling factor, which is 1 for a buried charge. To simulate a fully buried explosion, a 50 kg TNT spherical charge buried 5 m below the earth's surface is modeled in a 20 m × 20 m × 20 m soil domain. For the equivalent stand-off distance, *R*, the soil pressure predicted using the aforementioned empirical equation is plotted with the soil pressure acquired via FE simulation. Figure 3 shows strong agreement between the results, especially at larger stand-off distances.

Figure 3. Comparison of numerically determined soil pressure using the current numerical technique with pressure computed for a buried explosion using the TM5-855-1 empirical equation [29].

Additional validation is performed using ground-motion parameters, displacement, and PPA. Soheyli et al. [30] tested a small-scaled reinforced concrete tunnel with a box-shaped cross section (1 m × 1 m) and a wall thickness of 100 mm. A side-buried explosion of a 1.69 kg explosive (TNT-equivalent) situated 4 m from the tunnel wall was detonated and its effect on the tunnel was measured in terms of displacement and acceleration. This experimental setup is computationally replicated, and displacement and acceleration along the length of the wall facing the explosion are measured. Figure 4a,b shows a comparison between numerically derived and experimental data.

(**a**)   (**b**)
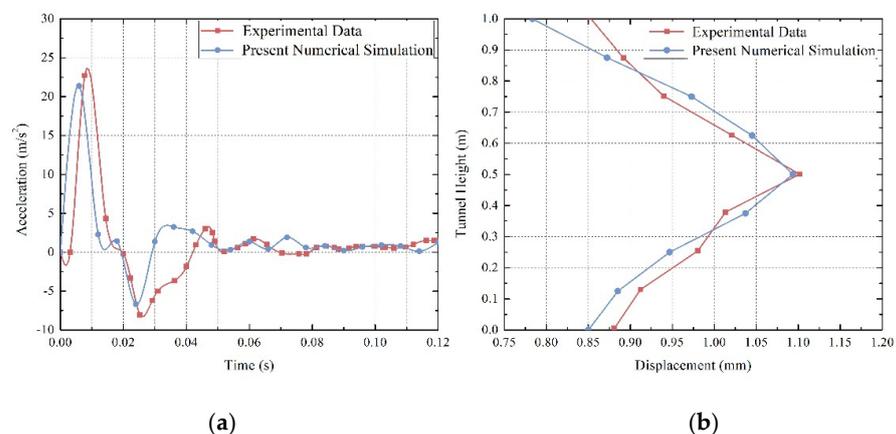
Figure 4. Comparison of numerically derived (**a**) acceleration and (**b**) displacement with experimental data [30].

5. Results and Discussions

The effect of a surface explosion of yield 200 kg TNT on the stability of tunnel is studied for all the geo-materials considered in the study. The crater formed on the topsoil layer made of sandy loam soil can be seen in Figure 5. When the entire geo-material domain consists of sandy loam soil, the apparent depth of the crater formed is 4.3 m. In the second case, the tunnel is surrounded by rock mass with a cover consisting of two different geo-materials, i.e., topsoil of 5 m thick sandy loam overlaying 1 m thick rock mass. For this case, the apparent depth of the crater is 3.45 m and it is found to be consistent for all types of rock considered. The two predominant causes behind crater formation during the surface explosion is shock-wave generation and rapid gas expansion. Both cause compression and erosion of geo-material in a radially outward direction. Compressive strength and toughness of sandy loam soil are significantly less than that of all rock types. The crater formation in the rock case stays constricted in the topsoil layer and is not extended into the rock layer. Hence, the crater formed in the first case is larger than that of the second case.
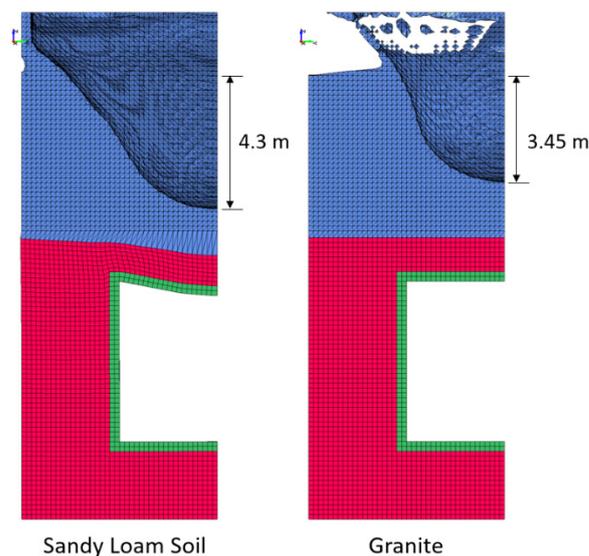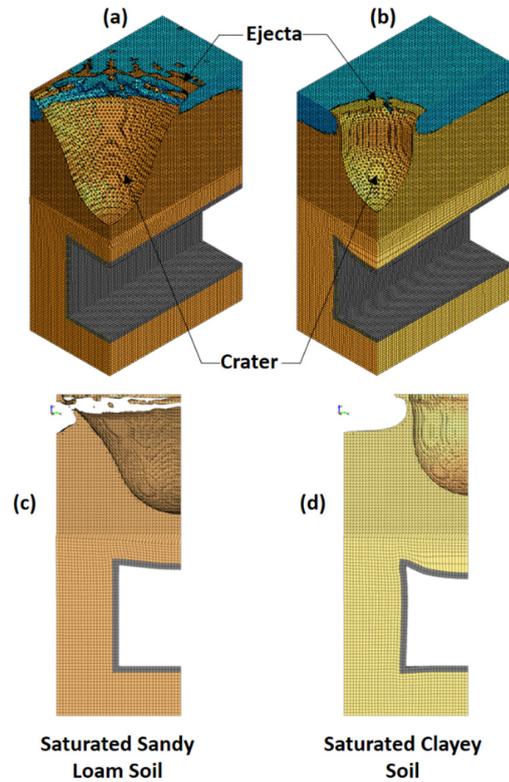

Figure 5. Crater formed due to surface explosion of yield 200 kg TNT in the cases of sandy loam soil and granite rock.

The blast-wave propagation and crater formation in sandy loam is compared with that of saturated clayey soil. The crater formed in sandy loam soil is wider and the side slope of the crater is flatter in comparison to the crater formed in clayey soil, as evident in Figure 6. The apparent size of the crater in sandy loam soil is relatively big, since the soil has larger air voids and is highly compressible in nature. Further, the shear strength of soil plays an important role in the development of craters as well. An increase in shear strength increases the side slope and depth-to-width ratio of the crater. The shear strength of clayey soil is considerably higher than that of sandy loam soil and, hence, a steeper side slope crater is observed. The clayey soil behaves comparatively stiffer and is less compressible. Since dissipation of blast energy due to compression is small, the tunnel roof suffers full collapse in the case of clayey soil.

It can be seen in Figure 7 that the deflection of tunnel lining is by far the highest for sandy loam soil compared to rocks. If the 1 m thick band of geo-material on top of the tunnel lining is considered as a beam, then the downward displacement measured at the tunnel crown can be taken as the center point deflection of the beam. The downward pressure exerted by the shock wave and gas expansion along with the surcharge of topsoil can be considered as the load acting on the beam, which is consistent for all cases of geo-material. Deflection of a beam is a function of beam stiffness which, in turn, depends on the strength characteristics of the material, especially the modulus strength. The smaller the modulus strength of the material, the higher the deflection of the beam will be. Revisiting

the material characteristics of the geo-material, it can be noticed that the shear modulus of all rock types considered is almost 9–10 times greater than the shear modulus of sandy loam soil. Thus, even though the attenuation capacity of sandy loam soil is higher than that of rock, it fails to mitigate the shock energy in the case of shallowly buried structures.


Figure 6. Crater formed due to surface explosion of yield 200 kg TNT: Isometric view of crater in (**a**) saturated sandy loam soil and (**b**) saturated clay; Side view of crater in (**c**) saturated sandy loam soil and (**d**) saturated clay.
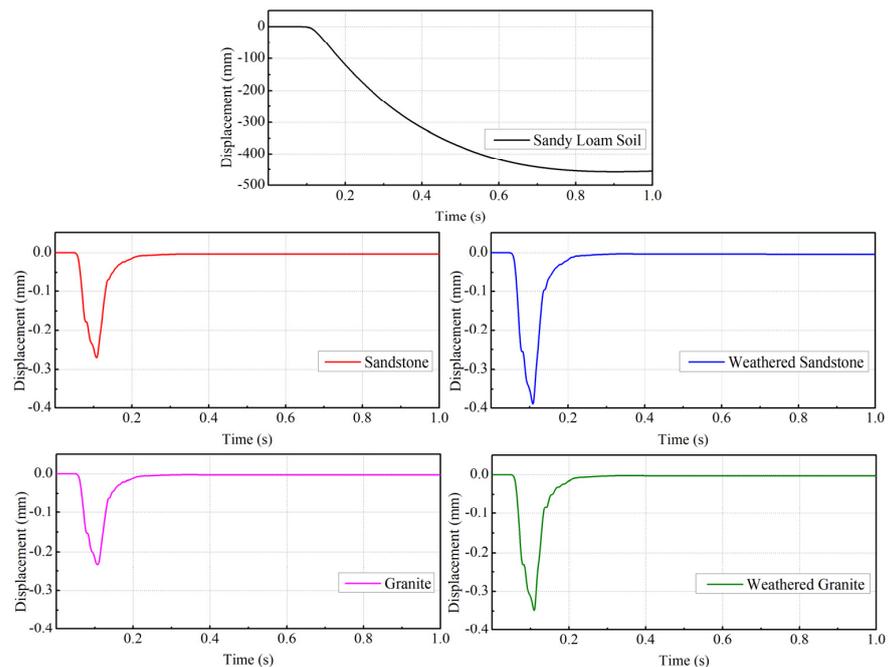
Figure 7. Displacement–time histories of tunnel buried in various geo-materials under surface explosion.

Negligible difference is observed between the deflections measured in sandstone and granite cases. The effect of the weathering of rock has also been briefly investigated. Although, compared to sandy loam soil, the deflections for weathered rock cases are much less, an increase in deflection of tunnel crown is observed when compared to intact rock for both sandstone and granite. Better visualization of the damage sustained by the tunnel due to the surface explosion is presented in Figure 8.
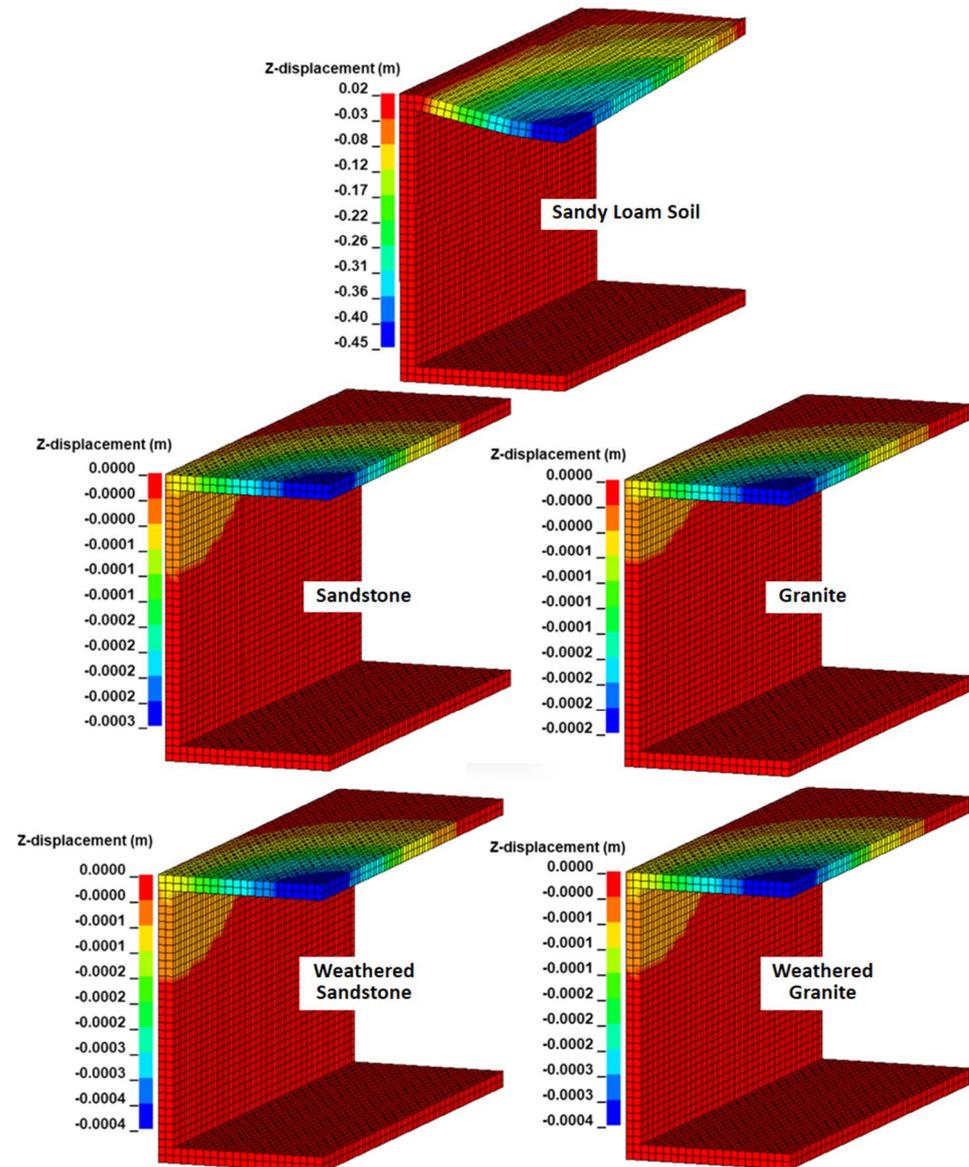
Figure 8. Displacement contour and deformed shape of tunnel under surface explosion for all geo-materials considered in the study.

The effect of water saturation on blast response of the tunnel has been studied and the displacement–time histories for each case of saturation level are compared in Figure 9. Maximum displacement is observed for case SL3 with the highest water saturation and least compressibility. Soil is a complex heterogeneous material, made up of a skeleton of weathered solid particles with pores filled with air and water. Initial theories assumed that soil particles did not undergo deformation; however, it was later verified that soil solids deformed under loading. Since water is known to be incompressible, the load is shared by the soil grain skeleton and water. Under a slow rate of loading, the water and air get expelled as the soil compresses. These assumptions worked well under static and quasi-static loading. However, under high-strain-rate loading such as blasts, water

does not get sufficient time to drain out during the loading period. The soil particles undergo deformations, and water and air get trapped in the soil skeleton. Water, being incompressible in nature, offers resistance against loading and does not allow compression of the soil matrix. Thus, when the water saturation in the soil increases, the compressibility of the soil decreases.
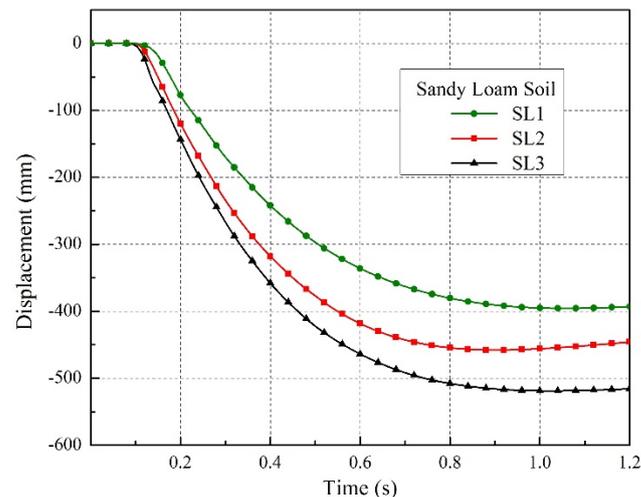
Figure 9. Displacement–time histories of tunnel buried in geo-material with varying degrees of saturation.

When the soil with a lower saturation level is loaded with a blast wave, compression of soil mass occurs due to the collapse of voids and the crushing of soil solids. The blast energy is partially utilized during compression of soil, which leads to attenuation of blast waves before it reaches the tunnel lining. However, when the saturation level is increased, the voids are filled with water, leading to decreased compressibility and attenuation. Thus, a large amount of impulse is transferred to the tunnel lining, which explains the highest displacement observed for soil case SL3.

6. Conclusions

The influence of geo-materials on the dynamic response of shallow-buried tunnels under surface explosions is investigated. Four geo-materials have been considered for the comparison: sandy loam soil, clayey soil, sandstone, and granite. An FE model of the problem is developed using the MM-ALE approach with help of software LS-DYNA®. Two consecutive aspects of surface explosions are studied, which are crater formation and shock-wave generation. The outcomes of the study are presented as follows:

1. The apparent depth of the crater is found to be higher in the case of sandy loam when compared to clayey soil and other rock types. On comparing the shape of craters between sandy loam and clayey soil, it was noticed that while sandy loam has a larger crater with a wider opening, the crater formed in clayey soil had a larger depth-to-width ratio with steeper side slopes;

2. The clayey soil behaved stiffer under the loading and did not undergo much compression compared to sandy loam soil. A large amount of blast energy was transferred to the tunnel structure. The tunnel sustains significant damage in the case of sandy loam soil; however, full collapse of tunnel roof is seen with saturated clayey soil. Sandy loam soil aided in dissipation of blast energy, resulting in a smaller degree of damage on the tunnel. Thus, a soil stratum composed of granular soil is more preferable than fine-grained soil for a loading condition as described in the study;

3. The deflection measured in the case of rocks is very small. The effect of weathering on the dynamic response of tunnels under blast load, although minute in comparison to that of sandy loam soil, is also observed. Higher deflection of tunnel crown is

measured in the cases of weathered counterparts of granite and sandstone when compared to the intact rocks. The damage can be minimized by adopting adequate tunnel support systems for tunnels constructed in highly weathered rocks;

4. The study concluded with a brief investigation of the effect of saturation. More impulse was transferred to the structure as the degree of saturation in soil was increased. The tunnel roof deflected the most in the case of sandy loam soil sample SL3 with the highest water saturation, implying that the presence of a high degree of moisture in soil can be detrimental to the stability of the tunnel. Prior to construction of tunnels under saturated soil conditions, the water table in the concerned region should be lowered by adopting a suitable dewatering method.

This study can be extended further by considering other types of geo-materials and different influential factors related to geo-materials.

Author Contributions: Conceptualization, J.M. and M.D.G.; methodology, J.M.; software, J.M.; validation, J.M.; formal analysis, J.M.; investigation, J.M.; resources, J.M. and M.D.G.; writing—original draft preparation, J.M.; writing—review and editing, J.M. and M.D.G.; visualization, J.M.; supervision, M.D.G. All authors have read and agreed to the published version of the manuscript.

Data Availability Statement: Not applicable.

References

1. Yang, Y.; Xie, X.; Wang, R. Numerical simulation of dynamic response of operating metro tunnel induced by ground explosion. *J. Rock Mech. Geotech. Eng.* **2010**, *2*, 373–384. [CrossRef]
2. Yankelevsky, D.Z.; Karinski, Y.S.; Feldgun, V.R. Re-examination of the shock wave's peak pressure attenuation in soils. *Int. J. Impact Eng.* **2011**, *38*, 864–881. [CrossRef]
3. Mobaraki, B.; Vaghefi, M. Numerical study of the depth and cross-sectional shape of tunnel under surface explosion. *Tunn. Undergr. Space Technol.* **2015**, *47*, 114–122. [CrossRef]
4. Mobaraki, B.; Vaghefi, M. Effect of the soil type on the dynamic response of a tunnel under surface detonation. *Combust. Explos. Shock. Waves* **2016**, *52*, 363–370. [CrossRef]
5. Mussa, M.H.; Mutalib, A.A.; Hamid, R.; Naidu, S.R.; Radzi, N.A.M.; Abedini, M. Assessment of damage to an underground box tunnel by a surface explosion. *Tunn. Undergr. Space Technol.* **2017**, *66*, 64–76. [CrossRef]
6. Mandal, J.; Agarwal, A.K.; Goel, M.D. Numerical Modeling of Shallow Buried Tunnel Subject to Surface Blast Loading. *J. Perform. Constr. Facil.* **2020**, *34*, 04020106. [CrossRef]
7. Mandal, J.; Goel, M.D.; Agarwal, A.K. Dynamic Response of Underground Tunnel in Soft Soil under Surface and Subsurface Explosion. *Pract. Period. Struct. Des. Constr.* **2022**, *27*, 04021081. [CrossRef]
8. Kumar, M.; Goel, M.D.; Matsagar, V.A.; Rao, K.S. Response of Semi-Buried Structures Subjected to Multiple Blast Loading Considering Soil–Structure Interaction. *Indian Geotech. J.* **2015**, *45*, 243–253. [CrossRef]
9. Karinski, Y.S.; Feldgun, V.R.; Racah, E.; Yankelevsky, D.Z. Mach stem due to an underground explosion near a rigid structure buried in soil. *Shock. Waves* **2015**, *25*, 63–76. [CrossRef]
10. Koneshwaran, S.; Thambiratnam, D.P.; Gallage, C. Performance of Buried Tunnels Subjected to Surface Blast Incorporating Fluid-Structure Interaction. *J. Perform. Constr. Facil.* **2015**, *29*, 04014084. [CrossRef]
11. Seyedan, M.J.; Seyedi Hosseininia, E. Significance of Soil Compaction on Blast Resistant Behavior of Underground Structures: A Parametric Study. *Civ. Eng. Infrastruct. J.* **2015**, *48*, 359–372. [CrossRef]
12. Rashiddel, A.; Kharghani, M.; Dias, D.; Hajihassani, M. Numerical study of the segmental tunnel lining behavior under a surface explosion—Impact of the longitudinal joints shape. *Comput. Geotech.* **2020**, *128*, 103822. [CrossRef]
13. Wu, T.; Jiang, N.; Zhou, C.; Luo, X.; Sun, J. Evaluate of anti-explosion for high-pressure gas steel pipeline subjected to ground explosion. *J. Constr. Steel Res.* **2021**, *177*, 106429. [CrossRef]
14. Qian, H.; Zong, Z.; Wu, C.; Li, J.; Gan, L. Numerical study on the behavior of utility tunnel subjected to ground surface explosion. *Thin-Walled Struct.* **2021**, *161*, 107422. [CrossRef]
15. Qu, Y.; Li, Z.; Zhang, R.; Qin, Y.; Zhang, D. Dynamic performance prediction and influencing factors analysis of buried polyethylene pipelines under subsurface localized explosion. *Int. J. Press. Vessel. Pip.* **2021**, *189*, 104252. [CrossRef]
16. Heydari, R.; Totonchi, A.; Ebrahimi, Z. Effect of the type of soil on the design criteria of horseshoe shape concrete structures under the surface blast. *Archit. Res.* **2017**, *7*, 201–211.
17. Jiang, N.; Gao, T.; Zhou, C.; Luo, X. Effect of excavation blasting vibration on adjacent buried gas pipeline in a metro tunnel. *Tunn. Undergr. Space Technol.* **2018**, *81*, 590–601. [CrossRef]

18. He, C.; Chen, D.; Xiao, J.; Lu, L.; Guo, Z. Experimental study of crack propagation and failure around a horseshoe tunnel during nearby blasting. *Int. J. Rock Mech. Min. Sci. Geomech.* **2021**, *139*, 104628. [CrossRef]
19. Mishra, S.; Kumar, A.; Rao, K.S.; Gupta, N.K. Experimental and numerical investigation of the dynamic response of tunnel in soft rocks. *Structures* **2021**, *29*, 2162–2173. [CrossRef]
20. Wang, G.; Cao, A.; Wang, X.; Yu, R.; Huang, X.; Lin, J. Numerical simulation of the dynamic responses and damage of underground cavern under multiple explosion sources. *Eng. Fail. Anal.* **2021**, *120*, 105085. [CrossRef]
21. Zhang, Z.; Zhou, C.; Remennikov, A.; Wu, T.; Lu, S.; Xia, Y. Dynamic response and safety control of civil air defense tunnel under excavation blasting of subway tunnel. *Tunn. Undergr. Space Technol.* **2021**, *112*, 103879. [CrossRef]
22. Busch, C.L.; Tarefder, R.A. Evaluation of Appropriate Material Models in LS-DYNA for MM-ALE Finite Element Simulations of Small-Scale Explosive Airblast Tests on Clay Soils. *Indian Geotech. J.* **2017**, *47*, 173–186. [CrossRef]
23. Wang, Z.; Zeng, Q.; Lu, Z.; Wan, L.; Zhang, X.; Gao, G. Numerical Simulation of Conical Pick Cutting Arc Rock Plate Fracture Based on ANSYS/LS-DYNA. *Adv. Mater. Sci. Eng.* **2020**, *2020*, e6563520. [CrossRef]
24. Lu, Z.; Zeng, Q.; Meng, Z.; Wang, Z.; Gao, G. Numerical Simulation on Cutting and Fracturing of Rock Plate with One Side Fixed and Three Sides Free. *Adv. Mater. Sci. Eng.* **2020**, *2020*, e2136297. [CrossRef]
25. Huang, J.; Zhang, G.; Luo, Y.; Hu, S.; Gong, H.; Li, X. Analysis of the Deformation Characteristics of the Surrounding Rock Mass a Deep Tunnel during Excavation through Fracture Zone. *Res. Sq.* **2021**. [CrossRef]
26. Yue, H.Z.; Yu, C.; Li, H.B.; Zhou, C.B.; Chen, S.H.; Shao, Z.S. The Effect of Blast-Hole Arrangement, Delay Time, and Decoupling Charge on Rock Damage and Vibration Attenuation in Multihole Blasting. *Shock. Vib.* **2022**, *2022*, e2110160. [CrossRef]
27. Wittmann, F.H.; Rokugo, K.; Brühwiler, E.; Mihashi, H.; Simonin, P. Fracture energy and strain softening of concrete as determined by means of compact tension specimens. *Mater. Struct.* **1988**, *21*, 21–32. [CrossRef]
28. Baker, W.E.; Westine, P.S.; Dodge, F.T. *Similarity Methods in Engineering Dynamics*; Elsevier: Amsterdam, The Netherlands, 1991.
29. U.S Army COE. *Fundamentals of Protective Design for Conventional Weapons*; TM 5-855-1; Technical Manual; Dept. of the Army: Washington, DC, USA, 1986.
30. Soheyli, M.R.; Akhaveissy, A.H.; Mirhosseini, S.M. Large-Scale Experimental and Numerical Study of Blast Acceleration Created by Close-In Buried Explosion on Underground Tunnel Lining. *Shock. Vib.* **2016**, *2016*, 1–9. [CrossRef]